Incorporating the Overmodulation Range in Space Vector Pattern Generators Using a Classification Algorithm

Alireza R. Bakhshai, Géza Joós, *Senior Member, IEEE,* Praveen K. Jain, *Senior Member, IEEE,* and Hua Jin, *Member, IEEE*

***Abstract*—Operating voltage-source pulsewidth-modulated (PWM) inverters in the overmodulation region extends their voltage and power ranges. Proper operation in this region is of particular importance in ac motor drives. This paper presents a classification algorithm for the implementation of the space vector modulation (SVM) in the pulse-dropping region. It is demonstrated that the proposed algorithm allows smooth transitions through the entire operating range up to square wave operation. It does not require approximations and guarantees exact positioning of the switching instants. In addition, it is shown that the harmonic distortion can be kept lower than with conventional techniques in most of the overmodulation region. The technique requires less computational time, when compared with the conventional SVM methods. The results of the theoretical and mathematical analysis are verified on a 2-KVA prototype unit using a digital signal processor (DSP)-based controller.**

***Index Terms*—Overmodulation, space vector modulation, three-phase inverter, voltage-source inverter.**

I. Introduction

FOR high-performance ac motor drive systems, full utilization of the dc bus voltage is an important factor in achieving maximum output torque under any operating condition, and extending the field weakening range of the motor. However, for a pulsewidth-modulated (PWM) voltage-source inverter (VSI), Fig. 1, employing subharmonic modulation (sinewave modulation), the maximum voltage is 78% of the six-step waveform value. Therefore, in general, a standard motor supplied from a PWM inverter is unable to operate at its rated voltage and power at rated speed [1]. To obtain sufficient voltage, operating the inverter in the overmodulation region is required.

The transition from a PWM wave to a six-step wave in conventional sine PWM is achieved by removing pulses from the PWM pattern until only a square wave remains. The disadvantage of this method, however, is that the dropping of pulses may result in a step change of the output voltage. Grant [2] analyzed the pulse-dropping problem from the view point of the proper pulse positioning to obtain a continuous output voltage, and concluded that the pulses should be symmetrically dropped from the leading and trailing edge of pulse pattern. However, there is no control on output distortion and increased output distortion results.

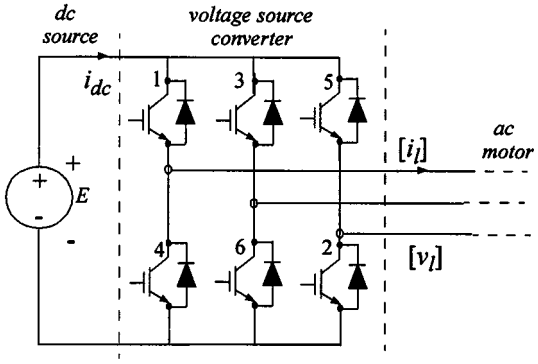

Fig. 1. Three-phase VSI topology.

Modulation strategies other than sine PWM were developed with the objective of delaying the onset of the pulse dropping. Among them, the third harmonic injection [3], and the space vector modulation (SVM) [4] are the more common approaches. By using either of these techniques the voltage utilization increases to 91% of the six-step value. However, above a certain terminal voltage level, any further increase in voltage results in a gradual decrease in the PWM switching frequency until the inverter produces a conventional six-step voltage. This pulse dropping phenomenon is inherent to the naturally sampled PWM technique. In addition, the gain in the transition region is nonlinear. Therefore, regardless of the modulation strategy, the dynamic characteristics of PWM inverters deteriorate with the transition to six-step operation [1], [2].

Currently, research in this area is focused on fully linearizing the inverter. Kerkman *et al.* extended the linearity of SPWM to six-step mode of operation by increasing the modulating command to the PWM in an inverse proportion to the decreasing gain [7], [8]. This is performed through a lookup table, and the method is adaptable to any PWM modulator. However, a lookup table requires a digital implementation, where the SVM is the best candidate for modulation strategy. Griva *et al.* [5] and Holtz *et al.* [6] proposed a technique by which switching times are calculated in the overmodulation region for a space vector modu-

Manuscript received March 24, 1998; revised June 23, 1999. Recommended by Associate Editor, S. Y. R. Hui.

A. R. Bakhshai is with the Department of Electrical and Computer Engineering, Isfahan University of Technology, Isfahan, Iran (e-mail: alireza@cc.iut.ac.ir).

G. Joós and P. K. Jain are with the Department of Electrical and Computer Engineering, Concordia University, Montreal, P.Q., H3G 1M8, Canada (e-mail: geza@ece.concordia.ca).

H. Jin is with the Department of Electrical Engineering, University of British Columbia, Vancouver, B.C., V6T 1Z4, Canada (e-mail: jinh@ee.ubc.ca).

Publisher Item Identifier S 0885-8993(00)00374-4.

lated inverter. The technique in [5] does not complete the transition to six-step operation, while in [6] this is done. In [9] and [10], a comparison between the Holtz techniques and the technique proposed in [7] is carried out.

SVM can be implemented using a classification technique [11]. The classification algorithm requires less computational effort, and as a result less computational time, when compared with the conventional SVM methods. This leaves more computational time for control purposes, or alternatively, allows higher switching frequency. The technique does not compromise accuracy and guarantees exact positioning of the switching instants. In [11], however, only the linear range of voltage control is discussed. Since the classification technique is significantly different from the conventional schemes, a different approach is developed to incorporate the overmodulation range.

This paper is a contribution to the implementation of overmodulation schemes for SVM. It extends the operating range of the classification algorithm to the pulse-dropping region. Two schemes, depending upon the output voltage level, are developed to continuously increase the output voltage, in a controllable manner, up to the maximum attainable value. It is demonstrated that these schemes are superior to existing techniques in terms of accuracy and computational requirements. The mathematical analysis is verified by means of experimental results obtained on a 2-KVA prototype unit using a digital signal processor (DSP)-based controller.

II. The SVM

SVM is a discrete type of modulation in which a sampled reference vector is synthesized by the time average of a number of appropriate switching state vectors. The reference and switching state vectors are represented in a complex plane by means of the α–β transformation

$$\begin{bmatrix} x_\alpha \\ x_\beta \end{bmatrix} = \begin{bmatrix} 1 & -1/2 & -1/2 \\ 0 & \sqrt{3}/2 & -\sqrt{3}/2 \end{bmatrix} \begin{bmatrix} x_a \\ x_b \\ x_c \end{bmatrix}. \tag{1}$$

This transformation when applied to the permitted switching states in a VSI, Fig. 1, results in six nonzero phase voltage space vectors ($\boldsymbol{V_K}$, $K = 1, 2, \cdots, 6$) forming a hexagon centered at the origin of α–β plane and two zero switching vectors ($\boldsymbol{V_7}$, $\boldsymbol{V_8}$) located at the origin of the plane (Fig. 2). The equation for the output voltage synthesis is [4]

$$V_r T = V_i t_i + V_{i+1} t_{i+1} + V_0 t_0 \tag{2}$$

where

T	cycle period;
V_r	reference voltage vector;
t_i, t_{i+1}, t_0	respective on duration of the adjacent switching state vectors (V_i, V_{i+1}, and V_0).

The on durations are defined as follows:

$$\begin{aligned} t_i &= mT \sin(60 - \theta) \\ t_{i+1} &= mT \sin(\theta) \\ t_0 &= T - t_i - t_{i+1}. \end{aligned} \tag{3}$$

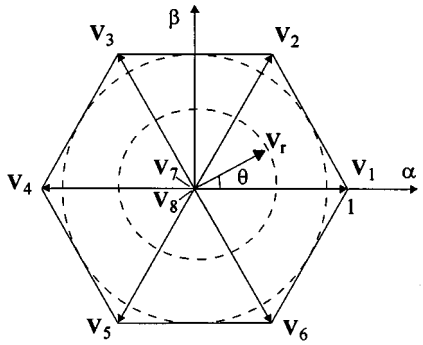

Fig. 2. Representation of the switching state vectors and input reference vector in the complex α–β plane.

The modulation index m is defined by

$$m = \left(2/\sqrt{3}\right) ||V_r||/E \tag{4}$$

where

E	dc bus voltage;
θ	angle between the reference vector V_r and the closest clockwise state vector (Fig. 2).

Based on Fig. 2, a reference voltage magnitude (rms) of 0.87 E corresponds to the maximum fundamental component of the output voltage obtained in the linear mode, that is $m = 1$. The six-step output corresponds to $m = 1.11$. The on-line implementation of the SVM requires that at every sample time, the sector where the space vector reference lies be established, the modulation index (m) calculated, and the on durations of the switching state vectors computed.

In conventional schemes, the magnitude and the phase angle of the reference voltage vector ($||V_r||$ and ϵ) are calculated at each sampling time and then substituted into (3) and (4). The required accuracy of the technique can be obtained by increasing the accuracy, thus the computation time, for sin and cos functions and thus producing a larger computing delay. Although the use of a lookup table and linear interpolation as a method of calculating and approximating reduces the computation time, interpolation of nonlinear functions may lead to reduced accuracy and therefore contribute to the deterioration of the PWM waveforms [13].

III. Classification Algorithm—Linear Mode

In [11], it has been shown that the SVM can be implemented by a simple and accurate algorithm based on classification techniques such as are found in neural network theory [12]. Fig. 3 shows a structural diagram of the algorithm. The reference vector is applied to a network composed of six calculating units, each unit being associated with it a predetermined gain vector. By selecting appropriate gain vectors, as shown in Fig. 3, the output of the kth unit is equal to the inner product of the reference vector and the kth switching state vector, that is,

$$n_k = ||V_r||\,||V_k|| \cos(\angle V_r, V_k), \qquad \text{for } k = 1, 2, \cdots, 6. \tag{5}$$

Assuming, without the loss of generality, that all are normalized, the inner product (5) can be rewritten as

$$n_k = ||V_r|| \cos(\theta_k). \tag{6}$$

Clearly, the closest V_k to V_r generates the largest n_k. Therefore, for example, if the reference vector V_r lies in the sector delimited by V_i and V_{i+1}, among all n_k, for $k = 1, 2, \cdots, 6$, n_i and n_{i+1} would have the largest positive values. Therefore, if a competitive network selects the two largest n_k, in this instance, n_i and n_{i+1}, the two switching vectors which contribute in synthesizing the output voltage are V_i and V_{i+1}.

The classification technique introduces an alternative to (6) to calculate n_k. Instead, the inner product between the reference vector V_r and a switching class vector V_k is simply obtained by a linear combination of the three voltage references, and determination of nonlinear functions involved in (6) are avoided, Fig. 3.

Regardless of the computation method, the output of the winner units are given by

$$\begin{bmatrix} n_i \\ n_{i+1} \end{bmatrix} = ||V_r|| \begin{bmatrix} \cos(\theta) \\ \cos(60-\theta) \end{bmatrix}. \tag{7}$$

In addition

$$\begin{bmatrix} \cos(\theta) \\ \cos(60-\theta) \end{bmatrix} = \frac{2}{\sqrt{3}} \begin{bmatrix} 1 & 0.5 \\ 0.5 & 1 \end{bmatrix} \begin{bmatrix} \sin(60-\theta) \\ \sin(\theta) \end{bmatrix}. \tag{8}$$

Substituting (8) in (7), and rewriting (7), we get

$$\frac{2}{3}\frac{T}{E} \begin{bmatrix} 2 & -1 \\ -1 & 2 \end{bmatrix} \begin{bmatrix} n_i \\ n_{i+1} \end{bmatrix} = m \begin{bmatrix} \sin(60-\theta) \\ \sin(\theta) \end{bmatrix} T. \tag{9}$$

The right side of (9) is the on duration of the adjacent switching state vectors V_i, and V_{i+1}, which now can equally be calculated from the left side of this equation as follows:

$$\begin{bmatrix} t_i \\ t_{i+1} \end{bmatrix} = \frac{2}{3}\frac{T}{E} \begin{bmatrix} 2 & -1 \\ -1 & 2 \end{bmatrix} \begin{bmatrix} n_i \\ n_{i+1} \end{bmatrix}$$

and

$$t_0 = T - t_i - t_{i+1}. \tag{10}$$

It is shown in [11] that by using this technique the implementation of the SVM requires less computation time and waveforms quality is improved due to better accuracy when compared to the traditional implementation techniques.

IV. Classification Technique—Overmodulation

This part of the paper shows how the classification technique can be extended to cover the overmodulation range. Fig. 4 shows the trajectory of the reference voltage space vector, which in the steady state is circular. As the modulation index increases, the radius of the circular trajectory in the linear region increases until at $m = M_1 = 1$ it becomes the circle inscribed by the hexagon. For this value of modulation index, the on duration of the zero vector reduces to zero when the reference vector touches the hexagon at $\theta = (2k+1)\pi/6$, where $k = 0, 1, \cdots, 5$. This is the upper limit of the linear modulation. Further increase in modulation index while keeping a circular trajectory necessitates negative duration of the zero vector(s), which is meaningless.

However, to achieve a higher output voltage, the modulation index can be further increased by programing the reference

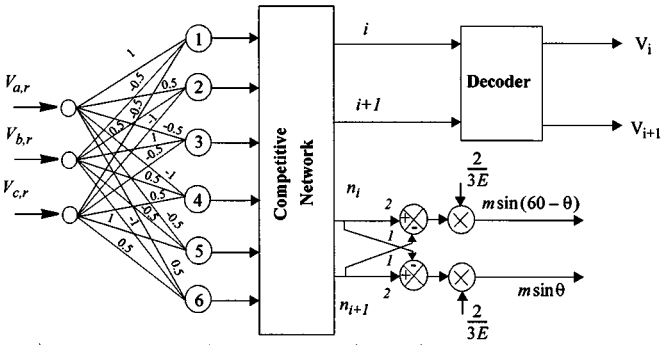

Fig. 3. Implementation of the SVM technique using a classification algorithm and incorporating the overmodulation region.

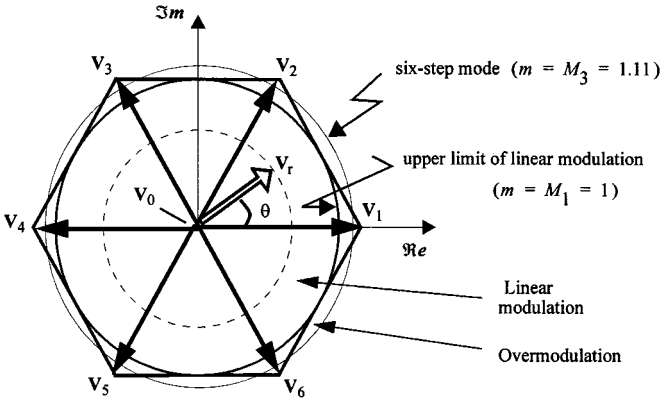

Fig. 4. Linear and overmodulation ranges in SVM.

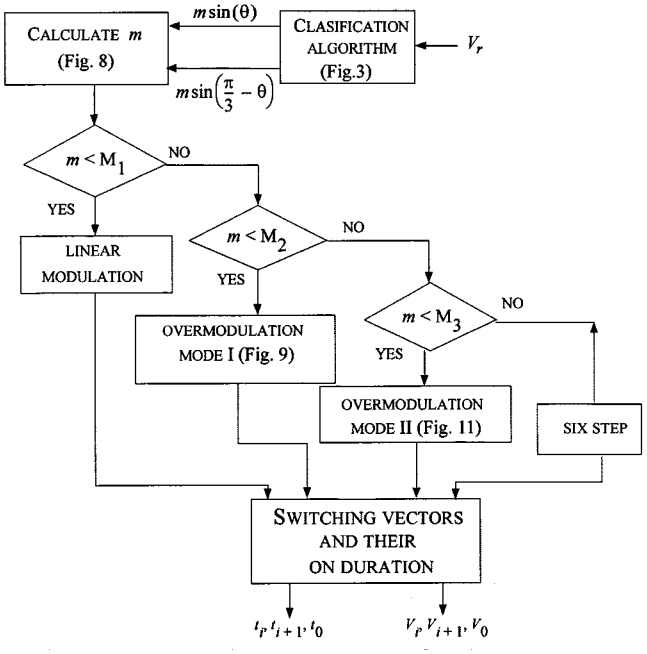

Fig. 5. Continuous transition from linear modulation to overmodulation in SVM technique.

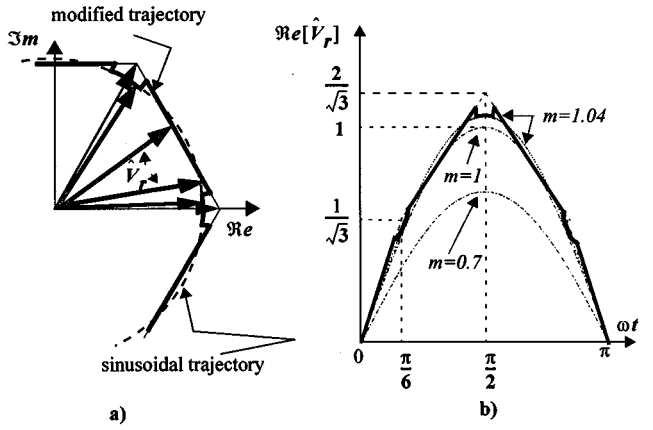

Fig. 6. Modified reference voltage vector in overmodulation mode I: (a) modified reference trajectory and (b) real component of the modified reference voltage.

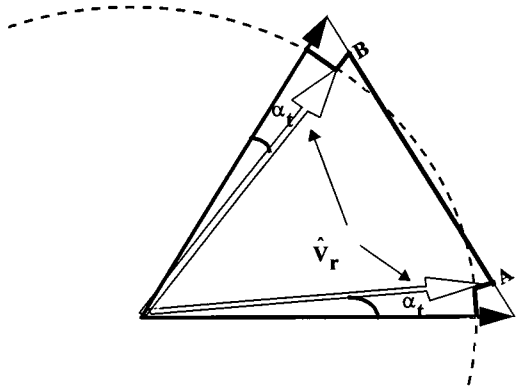

Fig. 7. Area over which an average for modulation index is given (overmodulation I, expanded from Fig. 6).

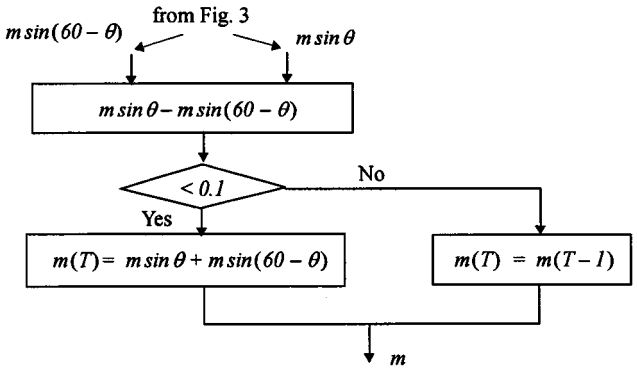

Fig. 8. Calculation of m in overmodulation regions I and II.

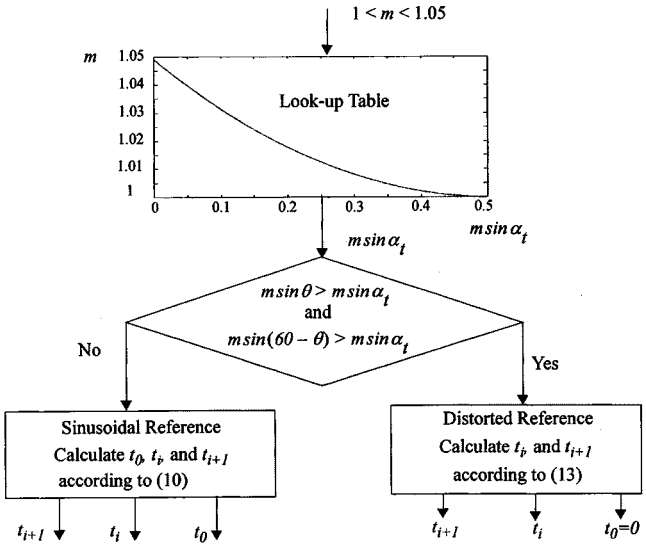

Fig. 9. Calculation of the on duration of the state vectors in overmodulation mode I.

voltage vector to smoothly deviate from a sinusoidal circular trajectory reaching ultimately a discrete six-step switching sequence. To keep a continuous control over the modulation index, and obtain the minimum distortion, the transition from the sinusoidal modulation to six-step operation is divided into two different modes, namely modes I and II. The maximum output voltage in modes I and II are obtained at $m = M_2 = 1.05$ and $m = M_3 = 1.1$, respectively. The complete procedure is depicted in the form of a flowchart in Fig. 5. In this flowchart, M_1 is the upper limit of the linear modulation, M_2 is the upper limit of the overmodulation mode I, and M_3 is the maximum attainable modulation index corresponding to the six-step operation. Based on the modulation index, the selector chooses among linear modulation, overmodulation mode I, and overmodulation mode II.

A. Overmodulation Mode I

In this range, the reference vector is distorted at a specific angle, and the distorted vector V_r is allowed to move along the hexagon side until the requested modulation index is obtained. The on duration of the zero vector is zero, as long as the end of this vector remains on the hexagon side. The maximum attainable modulation index in this mode of operation ($M_2 = 1.05$) is reached when the distorted reference vector remains on the hexagon side for all θ.

To get a smaller modulation index, in each sector, the reference vector follows a circular trajectory having a radius equal to the modulation index near the hexagon vertex. The inverter control selects the switching state vectors, and switches them according to (10). At a specific angle α_t, the reference vector is distorted and moves from the circular trajectory to the hexagon side and proceeds along it until reaches the point having the same distance from the next vertex. This compensates for that part of the circle (modulation index) which is outside the hexagon. A graphical interpretation of the control logic is shown in Fig. 6(a), where the modified trajectory is identified by thick lines. The distorted reference vector is shown in Fig. 6(b). When the end of the distorted reference voltage coincides with the hexagon, the on durations of the adjacent active switching state vectors add up to T, meaning that the on duration of the zero state vector becomes zero. This fact can be expressed by

$$t_i + t_{i+1} = T. \tag{11}$$

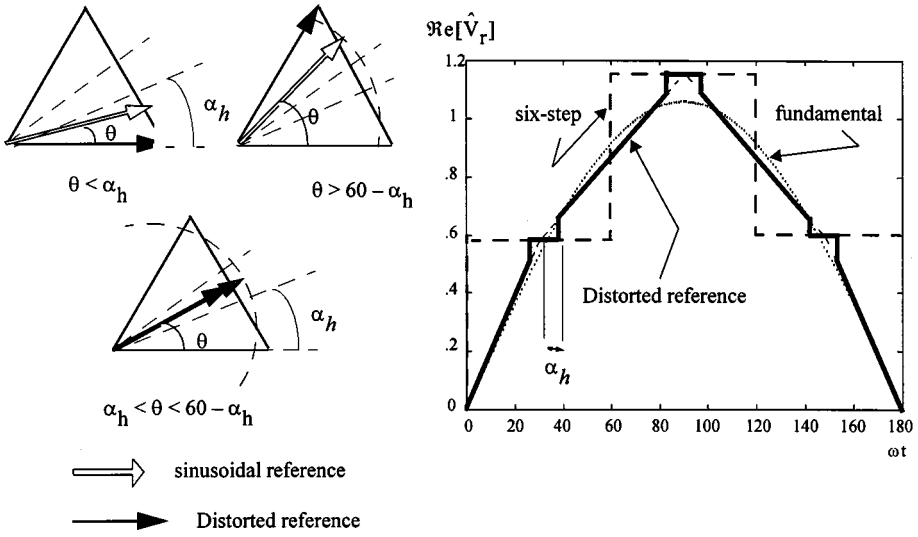

Fig. 10. Modification of the reference voltage in overmodulation mode II.

Replacing (3) into (11) gives

$$m = \frac{1}{\sin\theta + \sin(60-\theta)}. \tag{12}$$

For this m, the on durations of the adjacent active switching vectors are given by

$$\begin{aligned} t_i &= \frac{\sin(60-\theta)}{\sin\theta + \sin(60-\theta)}\,T \\ &= \frac{m\sin(60-\theta)}{m\sin\theta + m\sin(60-\theta)}\,T \\ t_{i+1} &= T - t_i. \end{aligned} \tag{13}$$

Equation (13) shows that with a little modification, the on duration of the adjacent active state vectors when the end of the reference voltage vector coincides with the hexagon, can be calculated from the outputs of the network in Fig. 3. If α_t is the voltage reference angle at which the transition from circular sinusoidal trajectory to the hexagon takes place, the average modulation index over AB in Fig. 7, therefore, can be calculated from

$$m = \frac{2}{(\pi/3 - 2\alpha_t)} \int_{\alpha_t}^{\pi/6} \frac{1}{\cos(\pi/6-\alpha)}\,d\alpha \tag{14}$$

which leads to

$$m = \frac{1}{2} \cdot \frac{1}{(\pi/6-\alpha_t)} \ln \frac{1+\sin(\pi/6-\alpha_t)}{1-\sin(\pi/6-\alpha_t)}. \tag{15}$$

The maximum attainable m in this mode of operation is 1.05 ($\alpha_t = 0$). The voltage reference angle α_t at which the trajectory must be translated to the hexagon for a specific value of m is calculated from (15). However, referring to the network in Fig. 3, and in order to maintain the simplicity of the classification algorithm, it is more convenient to calculate $m\sin\alpha_t$, and develop the algorithm based on this. Since at $\theta = 30°$, $m\sin\theta$, and $m\sin(60-\theta)$ are equal, the modulation index can easily be obtained from the addition of these two at $\theta = 30°$. For all other angles, m remains unchanged. Using this technique, the instantaneous modulation index will be modified six times during one period of the reference voltage. Fig. 8 shows the subroutine which provides an updated value for m at its output to be used in the general program of Fig. 5.

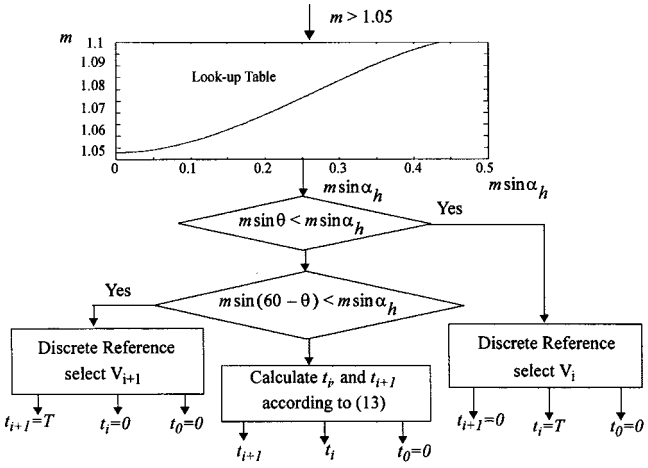

Fig. 11. Calculation of the on duration of the state vectors in overmodulation mode II.

Fig. 9 shows the operating principles of the converter in the overmodulation mode I. If m, calculated from the flowchart of Fig. 8, is less than M_2 and greater than M_1, the selector in the flowchart of Fig. 5 will select overmodulation mode I. In this mode, m as a function of $m\sin\alpha_t$ is calculated, and stored in the form of a lookup table. For a given value of m, the corresponding $m\sin\alpha_t$ can be reasonably approximated. A decision then is made based upon a comparison between the calculated $m\sin\alpha_t$, and the $m\sin\theta$ output of the network in Fig. 3. The on duration of the corresponding switching vectors then are calculated either from (10), end of reference vector on circular trajectory, or from (13), end of reference vector on the hexagon side.

B. Overmodulation Mode II

In this range, the modulation index further increases from $M_2 = 1.05$ to $M_3 = 1.1$ of the six-step maximum. The refer-

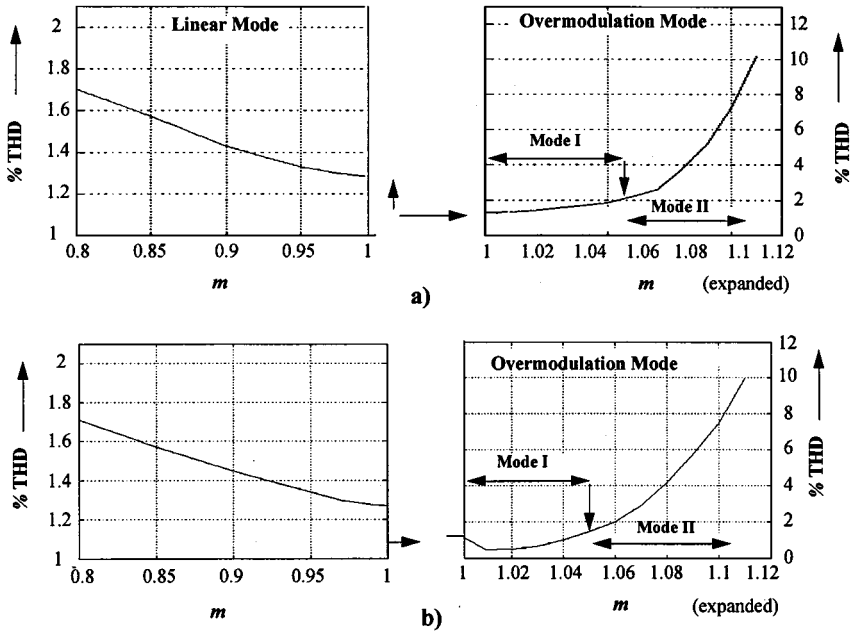

Fig. 12. Total current harmonic distortion versus modulation index: (a) constant cycle period and (b) constant switching frequency (reduced cycle period in overmodulation region).

ence voltage vector V_r is distorted in both magnitude and phase angle. The trajectory of the distorted reference vector jumps from a discrete six-step switching to a continuous hexagon side at a specific angle as shown in Fig. 10. In other words, V_r is held at a vertex for a particular time, and then moves along the hexagon side for the rest of the switching period. Such a switching method is identified by a hold angle α_h, which controls the time the distorted reference remains at the vertices. Fig. 10 shows the reference voltage and the distorted reference in both vectorial and real forms. It also indicates the time interval the distorted reference remains at the vertices for a preassumed hold angle. From the fundamental component of the distorted voltage shown in Fig. 10, the modulation index as a function of α_h is given by

$$m = \frac{4\sqrt{3}}{\pi^2}\left[2\alpha_h \cos\left(\frac{\pi}{6}-\alpha_h\right) + 2\sin\left(\frac{\pi}{6}-\alpha_h\right) + \alpha_h \cos\left(\frac{\pi}{6}+\alpha_h\right) - \sin\left(\frac{\pi}{6}+\alpha_h\right) + \alpha_h \sin\alpha_h + \cos\alpha_h\right]. \quad (16)$$

Fig. 11 shows the operating principles of the converter in the overmodulation mode II. If m calculated from the flowchart of Fig. 8 is less than M_3 and greater than M_2, the selector in the flowchart of Fig. 5 will select overmodulation mode II. In this mode, m as a function of $m \sin \alpha_h$ is calculated, and stored in the form of a lookup table. For a given value of m, the corresponding $m \sin \alpha_h$ can be reasonably approximated. A decision then can be made based upon a comparison between the calculated $m \sin \alpha_h$ and the current $m \sin \theta$ from the network in Fig. 3, and appropriate switching vectors are switched accordingly.

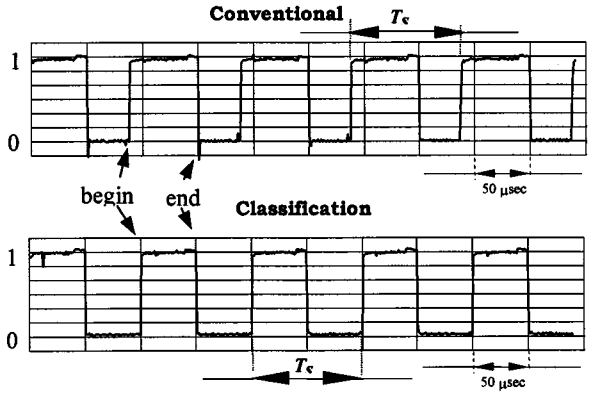

Fig. 13. Timing diagram showing the computing time in two different techniques.

V. Switching Frequency and Harmonic Distortion

In general, the current distortion can be reduced by increasing the switching frequency. Although the sampling frequency requirement of the SVM is far below the switching capability of the existing switching semiconductor devices [for example, insulated gate bipolar transistor (IGBT)], the switching speed is limited by the instruction execution speed and the minimum achievable interrupt interval of the microprocessor. Since additional computation time is required to incorporate the overmodulation range, the maximum attainable sampling frequency is further limited in this range. This justifies the use of the classification algorithm, which requires less execution time and provides accurate results in the overmodulation region.

The total current harmonic distortion is defined by

$$\%\text{THD} = 100 \times I_{s1'}\sqrt{\sum_{h=2}^{\infty} I^2 sh}. \quad (17)$$

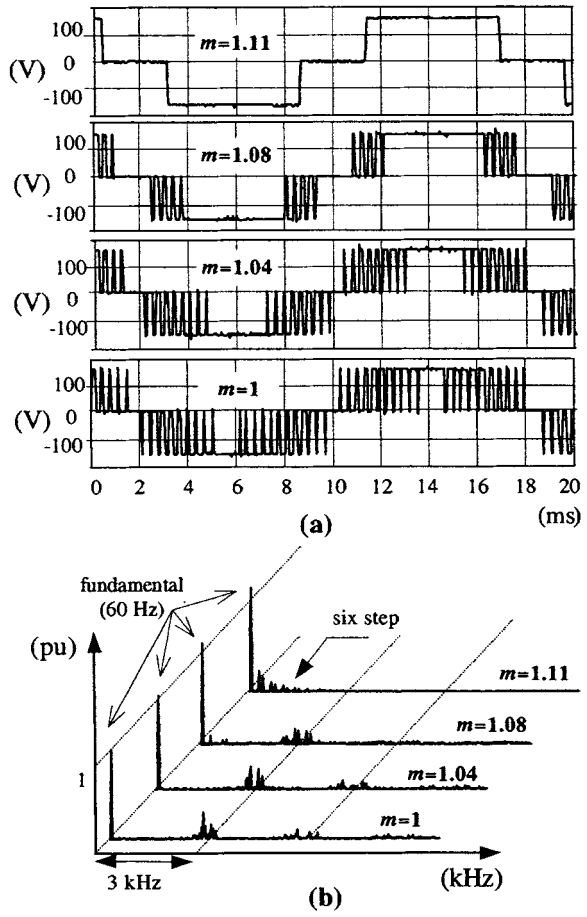

Fig. 14. Experimentally obtained line-line voltages and spectra in the overmodulation region (constant switching cycle): (a) line-to-line voltages and (b) spectra.

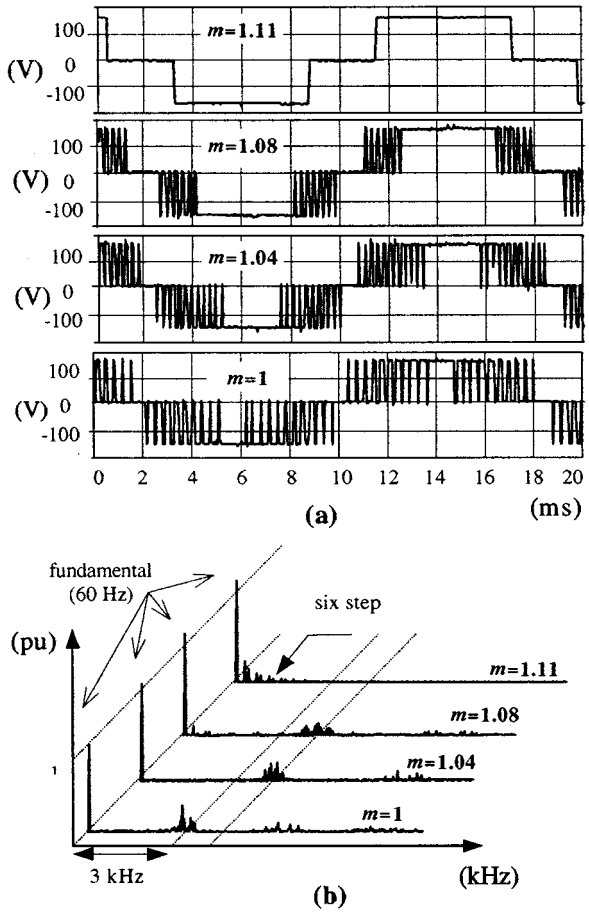

Fig. 15. Experimentally obtained line-line voltages and spectra in the overmodulation region (variable switching cycle): (a) line-to-line voltages and (b) spectra.

When the switching cycle for the whole range of modulation is kept constant, in the linear modulation range, the total current harmonic distortion decreases with the modulation index. However, less commutations per switching cycle obtained in the overmodulation range [see (3) and (13)], result in lower switching frequencies and higher distortion in the current waveforms. This effect is shown in Fig. 12(a), where the THD is drawn as a function of modulation index.

The impact of fewer commutations in the overmodulation region, however, can reduced by increasing the sampling rate. In the overmodulation mode I, when the distorted reference vector proceeds along the hexagon side, the switching cycle can be appropriately decreased to maintain a constant average switching frequency over a output cycle. This technique becomes less effective in the overmodulation mode II, and therefore in this region the harmonic distortion increases rapidly with the modulation index. Fig. 12(b) shows the total harmonic distortion (THD) is reduced considerably in overmodulation mode I by the appropriate selection of the switching cycle. Since the distorted reference vector in the proposed schemes coincides more with the hexagon when compared with its counterpart proposed by Holtz in both modes, lower harmonic distortion is obtained.

VI. Implementation Issues and Experimental Results

The proposed overmodulation schemes using a classification approach were implemented on a constant volt-per-hertz-controlled 2-KVA VSI laboratory setup. The prototype uses a TMS320C30 DSP microprocessor as the main controller without any additional hardware. To compare the computing time requirements of the DSP, both the proposed and the conventional approaches were implemented, and the timing diagram of Fig. 13 shows that 30% reduction is achieved by using the classification technique. It should be noted that this reduction is not obtained at the expense of accuracy. On the contrary, since in the classification algorithm, no function approximation is used to calculate the on duration of the switching state vectors, the results are more accurate than those obtained from the traditional implementation of the SVM [11].

For the first set of experimental results, the switching cycle was kept constant for the whole range of modulation index. Fig. 14(a) shows oscillograms of the line-to-line output voltages in the overmodulation range, and Fig. 14(b) shows the corresponding spectra. The impact of overmodulation on the effective switching frequency and the pulse-dropping effect can be clearly observed from this figure: low-order harmonics are gradually reintroduced.

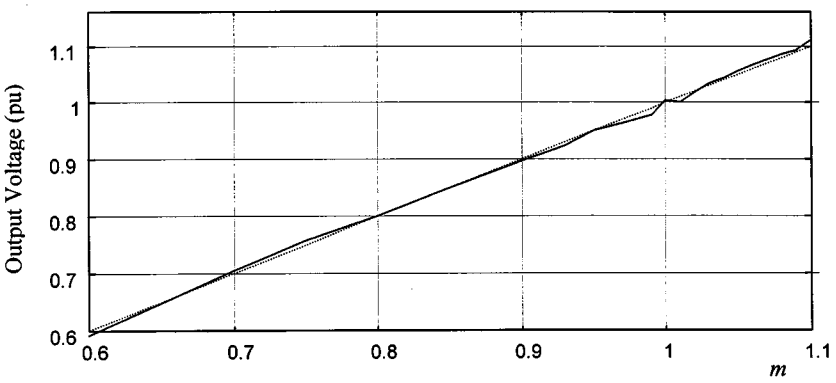

Fig. 16. Output voltage as a function of modulation index (measured). Linear relation shown as dotted line.

In the second set of experimental results, the switching cycle was reduced in the overmodulation regions, mode I and mode II, to compensate for the increased THD due to fewer commutations, as explained in Section V. Fig. 15(a) shows oscillograms of the line-to-line output voltages in the overmodulation range, and Fig. 15(b) shows the corresponding spectra. The THD is considerably reduced in overmodulation mode I, but only partially in overmodulation mode II, compared to the constant switching cycle case. Experimental results shown in Figs. 14 and 15 confirm the simulation results obtained in Fig. 12: by increasing the sampling rate in the overmodulation region, particularly in the overmodulation mode I region, the THD is improved.

The fundamental component of the output voltage as a function of the modulation index obtained experimentally is drawn in Fig. 16 (solid line). The dotted line corresponds to an ideal linear modulator. The effectiveness of the proposed schemes in continuously controlling the output voltage in the overmodulation region, while maintaining a linear characteristic, is thus demonstrated. Full utilization of the dc-bus voltage, therefore, is possible.

VII. Conclusions

In this paper, it has been demonstrated that the transition from a PWM waveform to a square waveform in SVM by pulse dropping can be performed using a classification algorithm. It has been verified experimentally that more accurate results with less computing time are obtained by using this technique in both linear and the linearized overmodulation range. The approach can be applied in a feedforward configuration or adapted to a closed-loop current control scheme.

When compared with other techniques, no function approximation is used to calculate the on duration of the switching state vectors in the overmodulation region. Furthermore, distortion of the reference vector in the overmodulation region is reduced, resulting in reduced output distortion. It can also be demonstrated that further reduction of the output distortion can be obtained by keeping the switching frequency constant using a variable switching cycle.

References

[1] D. A. Grant, "Techniques for pulse dropping in pulse-width modulated inverters," *Proc. Inst. Elec. Eng.*, pt. B, vol. 128, no. 1, pp. 67–72, 1981.

[2] ——, "Technique for pulse elimination in pulsewidth-modulation inverters with no waveform discontinuity," *Proc. Inst. Elec. Eng.*, pt. B, vol. 129, no. 4, pp. 205–210, 1982.

[3] J. A. Houldsworth and D. A. Grant, "The use of harmonic distortion to increase the output voltage of a three-phase PWM inverter," *IEEE Trans. Ind. Applicat.*, vol. IA-20, no. 5, pp. 1224–1228, 1984.

[4] W. Van der Brock, H. C. Skudelny, and G. Stank, "Analysis and realization of a pulse width modulator based on voltage space vectors," in *Conf. Rec. IEEE-IAS Annu. Meeting*, 1986, pp. 12–17.

[5] G. Griva, T. G. Habetler, F. Profumo, and M. Pastrelli, "Performance evaluation of a direct torque controlled drive in continuous PWM-square wave transition region," in *PESC'93*, pp. 237–244.

[6] J. Holtz, W. Lotzkat, and A. M. Khambadkone, "On continuous control of PWM inverters in the overmodulation range including the six-step mode," *IEEE Trans. Power Electron.*, vol. 8, no. 4, 1993.

[7] R. J. Kerkman, D. Leggate, B. J. Seibel, and T. M. Rowan, "An overmodulation strategy for PWM voltage inverters," in *IECON'93*, pp. 1215–1221.

[8] T. M. Rowan, R. J. Kerkman, and T. A. Lipo, "Operation of naturally sampled current regulators in the transition mode," *IEEE Trans. Ind. Applicat.*, vol. IA-23, no. 4, pp. 586–596, 1987.

[9] R. J. Kerkman, T. M. Rowan, D. Leggate, and B. J. Seibel, "Control of PWM voltage inverters in the pulse dropping region," *IEEE Trans. Power Electron.*, vol. 10, no. 5, pp. 559–565, 1995.

[10] A. M. Hava, R. J. Kerkman, and T. Lipo, "Carrier-based PWM-VSI overmodulation strategies, analysis, comparison, and design," *IEEE Trans. Power Electron.*, vol. 13, no. 1, 1998.

[11] A. Bakhshai, G. Joos, J. Espinoza, and H. Jin, "Fast space vector modulation based on a neurocomputing digital signal processor," in *APEC'97*, pp. 872–877.

[12] H. Hecht-Nielsen, *Neurocomputing*. Reading, MA: Addison-Wesley, 1990.

[13] S. Vukosavic and M. Stojic, "Reduction of parasitic spectral components of digital space vector modulation by real-time numerical methods," *IEEE Trans. Power Electron.*, vol. 10, no. 1, pp. 94–102, 1995.

Alireza R. Bakhshai received the B.Sc. and M.Sc. degrees from the Isfahan University of Technology, Isfahan, Iran, in 1984 and 1986, respectively, and the Ph.D. degree from Concordia University, Montreal, Canada, in 1997.

From 1986 to 1993, he was on the faculty of the Department of Electrical and Computer Engineering, Isfahan University of Technology. He was a Post-Doctoral Fellow from 1997 to 1998 at Concordia University. He is presently an Assistant Professor in the Department of Electrical and Computer Engineering, Isfahan University of Technology. His research interests include PWM techniques in medium and high power, FACTS devices, and active filters.

Géza Joós (M'78–SM'89) received the M.Eng. and Ph.D. degrees from McGill University, Montreal, Canada, in 1974 and 1987, respectively.

Since 1988, he has been an Associate Professor in the Department of Electrical and Computer Engineering, Concordia University, Montreal, where he is engaged in teaching and research in the area of power converters topologies and control. His present interests are the design and application of high-power converters to power system compensation, including FACTS and custom power devices. From 1975 to 1978, he was a Design Engineer with Brown Boveri Canada (now ABB) and involved in traction drives. From 1978 to 1988, he was a Professor at the Ecole de Technologie supérieure, Montreal, specializing in adjustable speed drives.

Dr. Joós is a member of the Industrial Power Converter Committee of the Industry Applications Society and is in charge of Special Activities. He is a registered Engineer in the Province of Quebec, Canada.

Praveen K. Jain (S'86–M'88–SM'91) received the B.E. (Hons.) degree from the University of Allahabad, India, and the M.A.Sc. and Ph.D. degrees from the University of Toronto, Toronto, Canada, in 1980, 1984, and 1987, respectively, all in electrical engineering.

Presently, he is a Professor at Concordia University, Montreal, Canada, where is engaged in teaching and research in the field of power electronics. Prior to this, he was a Technical Advisor with the Power Group, Nortel, Ottawa, Canada, where he was providing guidance for research and development of advanced power technologies for telecommunications. During 1987–1989, he was with Canadian Astronautics Ltd., Ottawa, where he played a key role in the design and development of high-frequency power conversion equipments for the Space Station Freedom. He was a Design Engineer and Production Engineer at Brown Boveri Company and Crompton Greaves Ltd., India, respectively, during the period of 1980–1981. He has published more than 100 technical papers and holds ten patents (with an additional ten pending) in the area of power electronics. His current research interests are power electronics applications to space, computer, and telecommunication systems.

Dr. Jain is a member of the Professional Engineers of Ontario and an Associate Editor of the IEEE TRANSACTIONS ON POWER ELECTRONICS.

Hua Jin (S'88–M'92) received the B.A.Sc. degree from Hunan University, China, in 1984 and the M.A.Sc. and Ph.D. degrees from the University of Toronto, Toronto, Canada, in 1987 and 1991, all in electrical engineering.

From 1991 to 1995, he was with the Department of Electrical and Computer Engineering, Concordia University, Montreal, Canada, as an Assistant Professor. Since 1995, he has been with the University of British Columbia, Vancouver, Canada. His research interest includes switch-mode power supplies, analog and digital control, and modeling and simulation of power electronics and motor drives.